THE JOURNAL OF PHYSICAL CHEMISTRY B

Article

Cite This: J. Phys. Chem. B 2019, 123, 2354−2361

pubs.acs.org/JPCB

Raman Spectroscopic Study of the Effect of Aqueous Salt Solutions on the Inhibition of Carbon Dioxide Gas Hydrates

Christine C. Holzammer[†,‡] and Andreas S. Braeuer*[,†]

[†]Institute of Thermal-, Environmental-, and Resources' Process Engineering (ITUN), Technische Universität Bergakademie Freiberg (TUBAF), 09599 Freiberg, Germany

[‡]Erlangen Graduate School in Advanced Optical Technologies (SAOT), Friedrich-Alexander-Universität Erlangen-Nürnberg (FAU), Paul-Gordan-Str. 6, 91052 Erlangen, Germany

ABSTRACT: We present an experimental Raman study on the thermodynamic inhibition effect of different salts (NaCl, KCl, $MgCl_2$, and $CaCl_2$ from 2.5 to 11 wt %) on the formation of carbon dioxide gas hydrates. We performed the experiments in a high-pressure vessel with two phases: a water-rich phase and a CO_2-rich phase. We investigated the changes the inhibitors induce in the water-rich phase before the onset of hydrate formation. This includes a study of the change in molar reaction enthalpy between strongly and weakly hydrogen-bonded water and the decrease in solubility of carbon dioxide in water. Additionally, the growth mechanisms of carbon dioxide hydrates were investigated by determining the amount of solid hydrates formed and the reaction constant. The results show that the molar reaction enthalpy, the solubility of CO_2, and the amount of solid hydrates formed can be correlated with the effective mole fraction, whereas the reaction constant is not affected by the addition of salts. The decrease of the molar reaction enthalpy can be directly correlated with the equilibrium temperature of the gas hydrates.

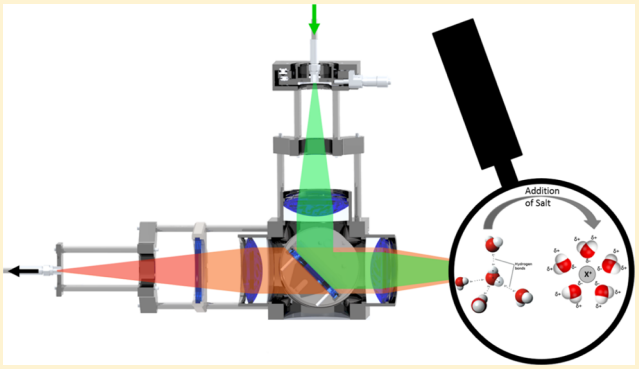

INTRODUCTION

Gas hydrates are solid crystals consisting of a hydrogen-bonded water network that is stabilized by incorporated guest molecules, such as hydrogen, carbon dioxide, or methane. Gas hydrates form at high pressures and low temperatures. In fields, where these conditions prevail, for example, gas gathering and conveyance, the prevention of unwanted formation of gas hydrates is of special interest as it can lead to pipeline blockage or destruction. For that reason, a wide variety of substances that impede the onset of gas hydrate formation, called inhibitors, were reviewed.[1] One group of inhibitors are thermodynamic inhibitors. They weaken the hydrogen-bonded network in the water-rich liquid phase before hydrate formation, leading to a shift of the gas hydrate formation conditions to lower temperature and higher pressure. To ensure safe operating conditions of pipelines, it is important to correctly estimate the temperature suppression that inhibitors induce in the system. The temperature suppression is the difference in temperature between the equilibrium temperature of gas hydrate formation without and with an inhibitor present. Many researchers have given correlations for temperature suppression in the literature: One of the first was proposed by Hammerschmidt[2] and is similar to the calculation of freezing point depression. It assumes that the temperature suppression is proportional to the weight fraction of the inhibitor in the aqueous phase. It is a good estimation for the temperature suppression of the thermodynamic inhibitors, methanol and glycol, but has to be modified for salts. An estimation for hydrate temperature suppression caused by salts was given by McCain.[3] This correlation is based on the gas specific gravity and the salt weight fraction. It gives good estimations for salinities smaller than 20 wt %, but the major drawback is that it does not account for the salt species. Especially the charge of the ions plays an essential role in the modification of the hydrogen-bonded network in the aqueous phase. Another correlation for predicting hydrate suppression temperatures was developed by Yousif and Young.[4] They expressed the hydrate suppression temperature as an empirical third-order polynomial, which is a function of the total mole fraction of the hydrate inhibitor in solution. The total mole fraction is calculated via the apparent molecular weight of salt in solution with salts. This is a function of the degree of ionization, which is different for different salts. However, Østergaard et al.[5] indicated that the correlation shows inaccuracies when tested on independent experimental data. Recently Hu et al.[6,7] established a universal correlation for the lowering of equilibrium temperature of gas hydrates by thermodynamic inhibitors. They showed that $\frac{T - T_0}{TT_0}$, where T_0 is the equilibrium

Received: November 14, 2018
Revised: February 14, 2019
Published: February 18, 2019

DOI: 10.1021/acs.jpcb.8b11040
J. Phys. Chem. B 2019, 123, 2354−2361

temperature without the inhibitor and T is the equilibrium temperature with the inhibitor, can be correlated with the effective mole fraction $X = \sum_{i=\text{ions}} |z_i| x_i$, where z_i is the charge of the dissolved salt ions and x_i is their mole fraction. We here analyze if the effective mole fraction can also be correlated with the properties of the liquid water-rich phase that lead to the depression of the equilibrium temperature. The properties of the liquid water-rich phase studied include the weakening of the hydrogen-bonded network [reaction enthalpy between strongly and weakly hydrogen-bonded (shb and whb) water molecules] and the solubility of carbon dioxide.

Another widely discussed topic in gas hydrate research is whether salts influence the kinetics of hydrate formation. Woo et al.[8] studied the formation of R22 gas hydrates in NaCl and $MgCl_2$ brines. In their experiments, both the growth constant and the overall gas uptake were significantly influenced by the presence of salts. This is in accordance with the work of Moeini[9] et al. who also found the overall gas uptake for CO_2 gas hydrates highly influenced by dissolved NaCl. On the other hand, Abay et al.,[10] who studied the formation of different synthetic natural gases, state that the kinetics of hydrate formation are not influenced by additives but only depend on the gas species. This is consistent with the work of Farhang et al.,[11] who found the growth rate of CO_2 gas hydrates with the addition of different sodium halides only slightly influenced. To contribute further insight into this dissent, we analyzed the influence of the hydrate formation inhibitors on the kinetics of hydrate formation and the amount of solid hydrates formed.

MATERIALS AND EXPERIMENTAL SECTION

The experiments were conducted with deionized water with a conductivity of less than 10 μS/cm, sodium chloride (NaCl, Alfa Aesar, optical grade), potassium chloride (KCl, Merck, Reag. Ph Eur), magnesium chloride ($MgCl_2$, Merck, ACS), calcium chloride ($CaCl_2$, Merck, ACS), and carbon dioxide (CO_2, Linde, molar purity 99.5%). For every salt concentration investigated, 100 mL of the corresponding solution was prepared with an analytical balance type ABJ-NM from Kern.

A sketch of the experimental setup is given in Figure 1. It can be divided into two parts: the Raman sensor head and the high-pressure view cell. The identical experimental setup is described in detail elsewhere, and only a brief description is given here.[12]

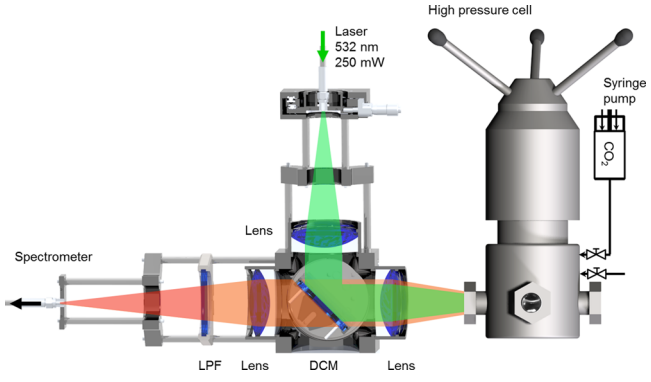

Figure 1. Sketch of the experimental setup consisting of the Raman sensor head with beam paths of excitation and the Raman signal and the high-pressure view cell; DCM stands for dichroic mirror and LPF stands for long pass filter.

The high-pressure view cell has four optical accesses and screw fittings for filling and emptying. For pressurization with CO_2, it is connected to a syringe pump. Temperature and pressure are monitored and recorded continuously throughout the experiment. The temperature is measured with a PT100 thermocouple class AA with a resolution of 0.05 K and an uncertainty of 0.12 K for the temperature range investigated. A pressure sensor type PAA-33X from Keller with a precision of 0.01 MPa (according to manufacturer specification) was used to monitor the pressure.

At the beginning of the experiment, the cell is flushed with CO_2. Afterward, 20 mL of the water/salt solution is filled into the cell, the pressure is set to 6 MPa by adding excess CO_2, and the temperature is set to 286 K. Under these conditions, a liquid CO_2-rich phase forms on top of a liquid water-rich phase, where all salt is dissolved in the liquid water-rich phase. Agitation with a magnet stick inside the chamber assures equilibration between the two phases (dissolution of CO_2 into the water-rich solution). As soon as the recorded Raman spectra indicate no further change, meaning that the intensity ratio of the Raman signals of CO_2 and water $\frac{I_{CO_2}}{I_{water}}$ is constant, equilibrium is reached. Then, the stirred system is cooled from 286 K at a rate of 3 K/h to a temperature, which is 1 K above the freezing temperature for the respective salinity. The freezing temperature was estimated using Blagden's law like in a previous work.[13] This corresponds to a subcooling (difference between the equilibrium temperature of hydrate formation and the set temperature) of all experiments between 9 and 9.5 K. When the final set temperature is reached, it takes between 1 and 7 h until spontaneous hydrate nucleation starts, and 30 min after that, no further hydrate is formed. This point is identified by no further changes in the shape of the Raman signal of the OH-stretching vibration. We refer to this as the end of hydrate formation.

The light source for the Raman sensor is a frequency-doubled Nd:YAG laser-type 532-250-AC from CNI that emits light with a wavelength of 532 nm and 250 mW. The beam is coupled with a fiber into the sensor head, where the divergent beam is collimated with a lens. Then, the beam hits a dichroic mirror (DCM), which is reflective for green light but transmittable for light with larger wavelengths. The beam is focused into the cell where light is scattered elastically and inelastically. The length of the measuring volume is approximately 5 mm (depth of field) and has a diameter of 0.2 mm. The inelastically scattered Raman signal is collected in a backscattering way. The signal can pass the DCM and is focused onto a fiber, which guides the light to a spectrometer QE65Pro from Ocean Optics, with an optical resolution of ~15 cm^{-1}. During each experiment, Raman spectra are gathered continuously from the start of cooling till the end of hydrate formation with an integration time of 1 s each and an acquisition rate of 1 spectrum/second. Every experiment was repeated three times. The error bars presented in the section Results and Discussion are the standard deviations from the repetition of measurements.

RESULTS AND DISCUSSION

Evaluating the Water-Stretching Vibration. The Raman signal of the stretching vibration of water, here referred to as the OH-stretching vibration, is well-known to be dependent on the development of hydrogen bonds.[14,15] It can be used to measure properties that influence the

DOI: 10.1021/acs.jpcb.8b11040
J. Phys. Chem. B 2019, 123, 2354−2361

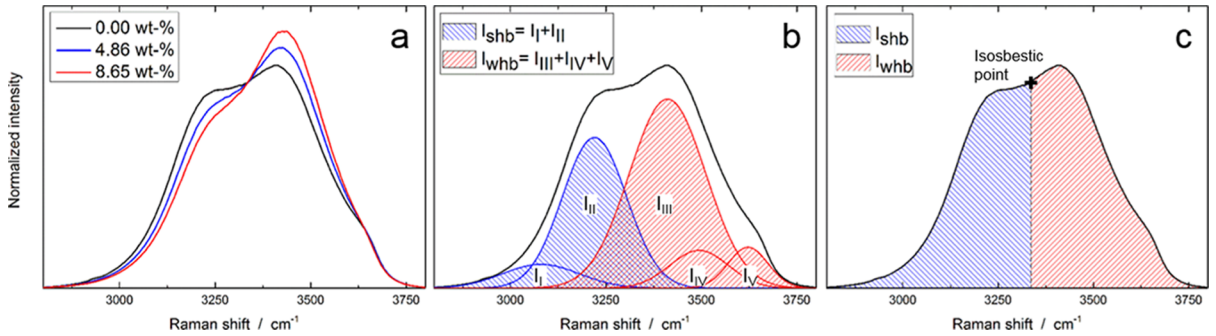

Figure 2. (a) Area-normalized Raman spectra of the OH-stretching vibration of liquid water from $MgCl_2$/water solutions at p = 6 MPa and T = 280 K. (b) decomposition of the Raman spectrum into five Gaussian peaks, (c) bisecting the Raman spectrum at the isosbestic point.

development of hydrogen bonds, such as temperature,[16] density, composition of a water-containing liquid mixture,[17] or the presence of hydrophobic surfaces.[18] The Raman spectrum of the OH-stretching vibration of liquid water is shown in Figure 2a for different mass fractions of dissolved magnesium chloride at a temperature of 280 K. All spectra are normalized to the integral of the Raman spectrum, or in other words, to their area. All spectra intersect at a Raman shift of 3337 cm^{-1}, the isosbestic point for the investigated systems. In the following, the region from 2800 to 3337 cm^{-1} will be referred to as the left shoulder and the region from 3337 to 3800 cm^{-1} as the right shoulder of the Raman spectrum of the OH-stretching vibration of water.

As the mass fraction of salt in the solution increases, the intensity of the right shoulder increases while the intensity of the left shoulder decreases. To explain this behavior, we can use a simplifying model of the water-rich phase that acts on the assumption of water molecules in two different states: shb water molecules and whb water molecules. Using that terminology, "weak" and "strong" applies to the number of hydrogen bonds a water molecule engages with its neighboring water molecules. It does not refer to the strength of one specific hydrogen bond. Accordingly, the left shoulder of the OH-stretching vibration can be attributed to shb water molecules and the right shoulder to whb water molecules. Consequently, the shape of the OH-stretching vibration is a measure for the development of the hydrogen-bonded network in water and thus is sensitive to influences that alter the hydrogen-bonded network, such as temperature or, as depicted in Figure 2a, salinity.

The alteration of the shape of the OH-stretching vibration generated by the salt can be explained as follows: Salt is dissolved in water by the formation of a hydration shell of water molecules around the charged salt ions. The interaction of salt ions and water is governed by Coulombic forces, which are much stronger than the interaction of two water molecules that interact via hydrogen bonds. Therefore, the hydrogen-bonded network is disturbed, meaning that more water molecules are whb.

To quantify the change of shape of the OH-stretching vibration, the van't Hoff behavior can be utilized

$$\left(\frac{\partial \ln k}{\partial \frac{1}{T}}\right)_p = -\frac{\Delta_R h^0}{R} \tag{1}$$

In the classic approach, the van't Hoff equation describes an equilibrium reaction, in which k is the equilibrium constant, T is the temperature, R is the universal gas constant, and $\Delta_R h^0$ is the standard molar reaction enthalpy. There are different opinions in the literature as how to use this equation in relation to the temperature-dependent shape of the OH-stretching vibration of water.

Some take the existence of an isosbestic point as an indication for equilibrium between two components, here, shb and whb water molecules.[19,20] Others state that this behavior arises from a continuous thermally equilibrated distribution.[21,22] The first group usually decomposes the spectrum typically into five Gaussian peaks (some use a different number of peaks), which can be assigned to different local hydrogen bondings, referring to the interaction of one water molecule with its neighbors. This method is shown in Figure 2b. Afterward, the intensity of shb water molecules is the sum of the first two peaks (whose central wavenumbers are left to the isosbestic point) and the one of whb water molecules is the sum of the three peaks with higher Raman shifts (whose central wavenumbers are right to the isosbestic point).[23]

$$k = \frac{I_{shb}}{I_{whb}} = \frac{I_I + I_{II}}{I_{III} + I_{IV} + I_V} \tag{2}$$

A variation of that method is to build the ratio between two peaks, for example, Peak 1 and Peak 5, $k = \frac{I_{shb}}{I_{whb}} = \frac{I_I}{I_V}$, as Peak 1 is assigned to fully hydrogen-bonded water molecules and Peak 5 to non-hydrogen-bonded water molecules.[24]

The second group objects and holds the opinion that the decomposition of the spectrum into peaks is unjustified as there are no distinct populations.[21] Nevertheless, according to them, the spectrum can be divided at an arbitrary point, and the ratio of the two areas will give the difference in the average energy between the two subensembles of shb and whb water molecules.[22] This method is illustrated in Figure 2c.

When fitting the OH-stretching with five Gaussians (Figure 2b), the choice of the initial parameters and their limits will affect the results greatly. A Gaussian peak $g(\bar{\nu}_R)$ is represented by the formula

$$g(\bar{\nu}_R) = \frac{h}{\sigma\sqrt{2\pi}} \exp\left[-\frac{1}{2}\left(\frac{\bar{\nu}_R - \bar{\nu}_{R,central}}{\sigma}\right)^2\right] \tag{3}$$

with three free parameters, the height h, the standard deviation σ, and the central Raman shift $\bar{\nu}_{R,central}$. Consequently, as there are 5 peaks, there are 15 parameters for each fit. If all of them are left free for each fit, the residual of the fit is very small, although the smooth change of the OH-stretching vibration with temperature is not represented by a smooth change in the intensities of the five peaks with temperature. On the contrary,

DOI: 10.1021/acs.jpcb.8b11040
J. Phys. Chem. B 2019, 123, 2354−2361

if two parameters for each Gaussian are set, the choice of the right values that are feasible for all spectra at different temperatures and salinities is difficult. Inappropriate values lead to a smooth change in the intensities of the peaks with temperature but high residuals of the fit. For that reason, we performed our fit in the following way: All parameters were left free, but the central Raman shifts for the five peaks and their respective standard deviation had to be the same for all spectra, whereas the height of the peaks is individual for each spectrum. Table 1 lists the results of the fit, which are in good agreement with the spectra in the investigated temperature and salinity range. The peak fitting was performed with a custom program written in Matlab R2017b.

Table 1. Wavenumbers of the Central Raman Shift and Standard Deviations of the Five Fitted Gaussian Peaks of the Decomposed OH-Stretching Vibration

peak number	central Raman shift $\bar{\nu}_{R,central}/cm^{-1}$	standard deviation σ/cm^{-1}
I	3079.8	100.7
II	3220.2	84.0
III	3411.5	100.1
IV	3493.9	76.6
V	3622.3	52.2

The values of the molar reaction enthalpy calculated are shown in Figure 3. $\Delta_R h^0$ is negative for all salt concentrations. Depending on whether the equilibrium constant is defined as $k = \frac{I_{shb}}{I_{whb}}$ or vice versa, negative or positive values result. Here, it is the ratio of shb water molecules and whb water molecules. Thus, it can be concluded that the enthalpy of shb water molecules is less than that of whb water molecules. This is expected, as the potential energy of shb water molecules is smaller than that of whb water molecules because of the higher development of hydrogen bonds. With increasing salinity, the absolute value of $\Delta_R h^0$ decreases, as water molecules form a hydration shell around salt ions, and the hydrogen-bonded network is weakened. In previous studies[12,25] of sodium chloride solutions, it was shown that $\Delta_R h^0$ shows a linear correlation with the mass fraction of dissolved NaCl. In our results presented here for different salts, it can be seen that $\Delta_R h^0$ correlates well with the effective mole fraction for all four different salts. This shows that the weakening is not only influenced by the amount of salt in the solution but also by the charge of the respective salt. The size of the cations seems to play a minor role as this property is not considered in the effective mole fraction, and no significant difference between cations in the same group of the periodic table can be detected.

Figure 3a compares the values of $\Delta_R h^0$calculated with the two methods: decomposition into five Gaussians (according to Figure 2b) and bisecting at the isosbestic point (according to Figure 2c). The two methods provide different absolute values but show the same trend. Figure 3b shows $\Delta_R h^0$ scaled to the respective value of pure water $\Delta_R h^0_{water}$. For that, both methods result in the same relation: the molar reaction enthalpy decreases linearly with the effective mole fraction to approximately 70% of the one without salt for an effective mole fraction of 0.08.

This result suggests that using the OH-stretching vibration and van't Hoff's relation is not suitable for determining a specific value of $\Delta_R h^0$ for a hydrogen bond. However, it is applicable for a qualitative prediction of the development of the hydrogen-bonded network in an aqueous solution.

As the molar reaction enthalpy $\Delta_R h^0$ correlates well with the effective mole fraction and as the depression of the hydrate equilibrium temperature in the form $\frac{T - T_0}{TT_0}$ can also be correlated with this quantity,[6] we correlated $\frac{\Delta_R h^0}{\Delta_R h^0_{water}}$ with the hydrate equilibrium dissociation temperatures shown in Figure 4. The hydrate equilibrium dissociation temperatures were calculated with the relation given from Hu et al.[6]

It can be seen that the relative molar reaction enthalpy $\frac{\Delta_R h^0}{\Delta_R h^0_{water}}$ correlates well with the equilibrium dissociation temperature $T_{dissociation}$. With that, we show that the depression of the equilibrium dissociation temperature is a result of the weakening of the hydrogen-bonded network from the addition of salt.

Evaluation of the Solubility of CO_2. In a previous work,[13] we showed that in a CO_2 and water mixture, the ratio of the Raman signal of CO_2 and water in the liquid water-rich phase is directly proportional to the amount of CO_2 dissolved in the liquid water-rich phase and the amount of water contained in the water-rich liquid phase

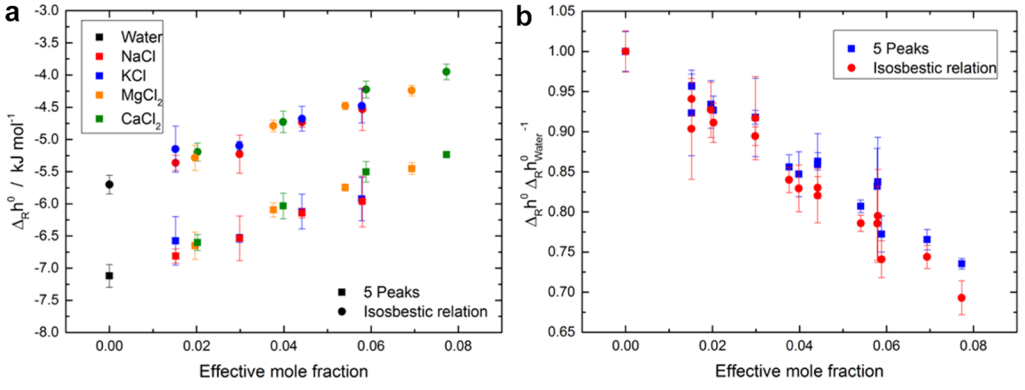

Figure 3. (a) Standard molar enthalpy $\Delta_R h^0$ as a function of the effective mole fraction for the decomposition of the spectrum into five Gaussians peaks (squares) and bisecting at the isosbestic point (circles). (b) Standard molar enthalpy $\Delta_R h^0$ normalized to the standard molar enthalpy of water $\Delta_R h^0_{water}$ as a function of the effective mole fraction for decomposing the spectrum into five Gaussian peaks (squares) and dividing the spectrum at the isosbestic point (circles).

DOI: 10.1021/acs.jpcb.8b11040
J. Phys. Chem. B 2019, 123, 2354−2361

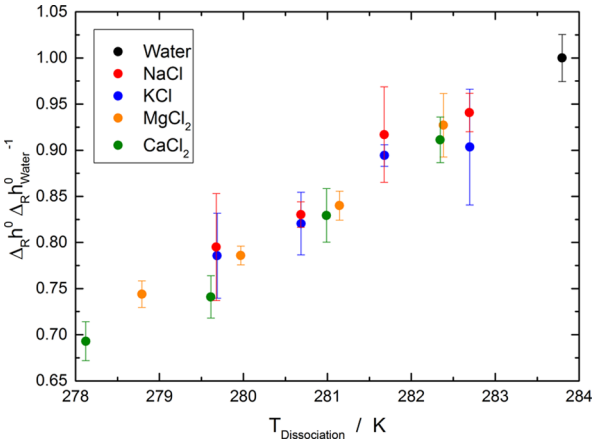

Figure 4. Standard molar enthalpy $\Delta_R h^0$ normalized to the standard molar enthalpy of water $\Delta_R h^0_{water}$ as a function of the equilibrium dissociation temperatures $T_{dissociation}$ of hydrate.

$$\frac{I_{CO_2}}{I_{water}} = a\frac{n_{CO_2}}{n_{water}} = a \cdot S \tag{4}$$

with a being the proportionality constant.

To determine the constant a, we measured the intensity ratio $\frac{I_{CO_2}}{I_{water}}$ at conditions with known solubility values $S = \frac{n_{CO_2}}{n_{water}}$ from the literature.[26−28] The exact values from calibration are given in the supporting information of a previous paper,[13] with which the proportionality constant was calculated to be a = 2.76.

Figure 5a shows the molar ratio of CO_2 and water in aqueous $MgCl_2$ solutions with temperature. The data were gathered during the cooling period (temperature ramp of 3 K/h). It can be seen that the solubility of CO_2 increases with decreasing temperature because the solvation of CO_2 in water is exothermic.[29,30] As the solubility decreases linearly with approximately the same slope for the temperature range investigated, Figure 5b shows only the solubility at a temperature of T = 286 K for reasons of clarity. The solubility $S = \frac{n_{CO_2}}{n_{water}}$ for different effective mole fractions is scaled to the solubility of CO_2 in water without salt S_0.

The effective mole fraction seems to correlate with the solubility rather well, although a linear correlation would underestimate the solubility of carbon dioxide in KCl solution and overestimate the one in $MgCl_2$ solution.

This can be explained by the fact that the effective mole fraction takes the charge of the ions into account but not their size. As potassium and sodium are both monovalent and K^+ is bigger than Na^+, the electric field of sodium ions is stronger than that of potassium. Therefore, more water molecules are attracted to the sodium ion than to the potassium ion, leading to more water molecules in the hydration shell and less water molecules available for the dissolution of carbon dioxide. This causes a higher solubility of carbon dioxide in aqueous KCl solutions compared to NaCl solutions, with the same effective mole fraction of salt and accordingly a greater solubility in $CaCl_2$ solutions than in $MgCl_2$ solutions.

Evaluation of the Amount of Hydrate Formed and the Kinetics of Hydrate Formation. To determine the molar fraction of the solid hydrate formed, we used the method presented elsewhere,[13] and only a short description is given here. In the previous work, we used a ratio of scattering cross-sections of ice and hydrate from Slusher and Derr[31] for the calculations. In the meantime, new values for the scattering cross-sections were published by Plakhotnik and Reichardt;[32] nevertheless, in this work presented, we used the same values as for the previous paper.

The basic idea is that a hydrate gel forms in the cell, meaning a solid hydrate phase with liquid water occlusions inside. Therefore, the Raman signal from that gel is a superposition of the Raman signals of liquid water and solid hydrates. As their respective OH-stretching vibrations differ considerably, it is possible to decompose the signal from the hydrate gel in its contributions, attributable to the solid hydrate and to the liquid water. The spectra can be seen in Figure 6a.

Mathematically expressed, it results in

$$I^0_G(\bar{\nu}) = I^0_L(\bar{\nu}) \cdot x_L + I^0_H(\bar{\nu}) \cdot x_H \tag{5}$$

The spectrum of the hydrate gel $I^0_G(\bar{\nu})$ is a linear combination of the spectrum of liquid water $I^0_L(\bar{\nu})$ times the molar fraction of liquid water x_L and the spectrum of the solid hydrate $I^0_H(\bar{\nu})$ multiplied with the molar fraction of the solid hydrate x_H. In this connotation, the superscript 0 indicates the area-normalized spectra. This relation is evaluated for the Raman shifts $\bar{\nu}$ of the OH-stretching from 2800 to 3800 cm^{-1}, and x_H and x_L have to sum up to one.

Because of the continuous acquisition of Raman spectra, the evolution of the molar fraction of the solid hydrate formed x_H can be extracted, as can be seen in Figure 6b.

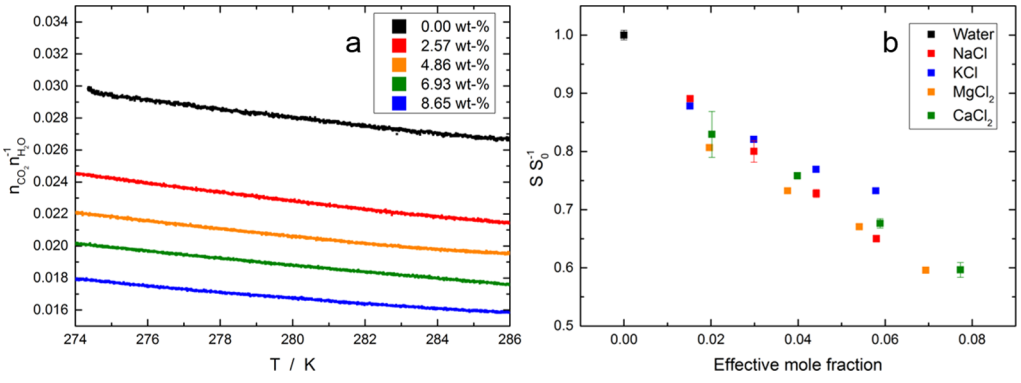

Figure 5. (a) Solubility of CO_2 in $MgCl_2$ solutions as a function of temperature and (b) solubility S of CO_2 in aqueous salt solution normalized to the solubility of CO_2 in water without salt S_0 at T = 286 K and p = 6 MPa.

DOI: 10.1021/acs.jpcb.8b11040
J. Phys. Chem. B 2019, 123, 2354−2361

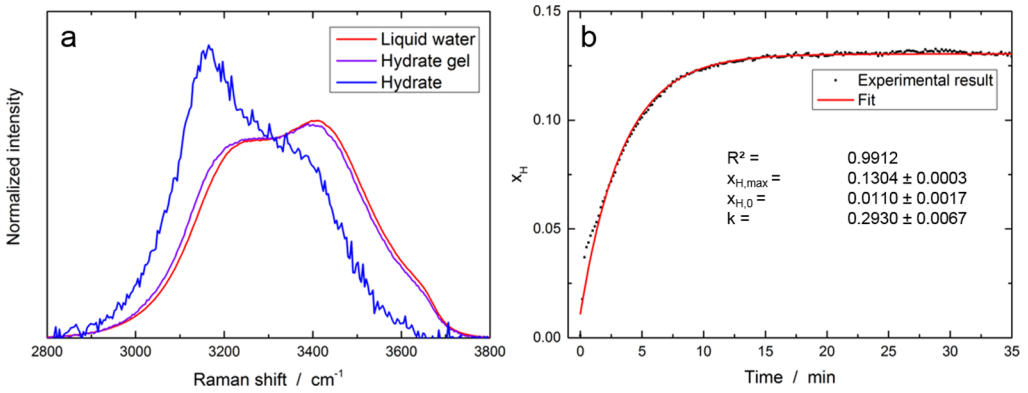

Figure 6. (a) Raman spectra of the OH-stretching vibration of water from the liquid water-rich phase, the hydrate gel, and the pure hydrate phase and (b) evolution of the molar fraction of the hydrate during formation with the best fit.

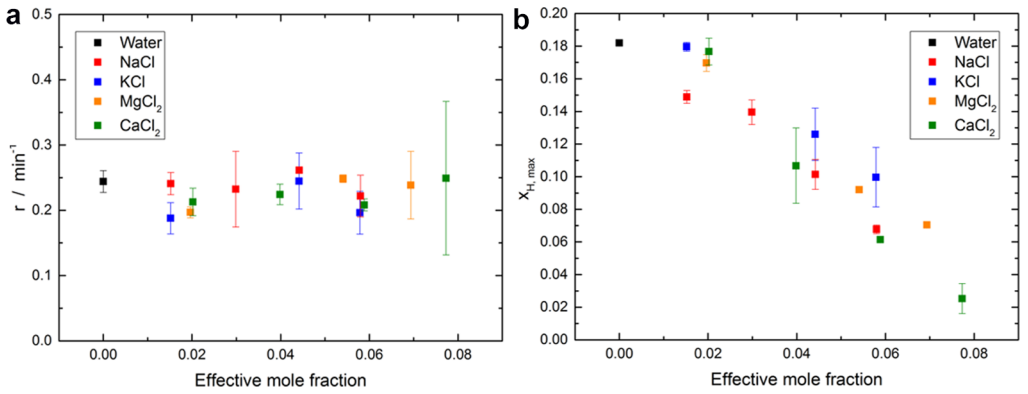

Figure 7. (a) Growth constant r and (b) molar fraction of the solid hydrate contained in the hydrate gel for different effective mole fractions of the dissolved salt.

Several models for the growth of gas hydrates have been proposed in the literature, considering different aspects of the three major correlations for hydrate growth: intrinsic growth kinetics, mass transfer limitation, and heat transfer limitation.[33] Strong agitation of the system can overcome mass transfer limitation.[8,34] For a relatively small reactor with sufficient cooling, the heat transfer limitation does not affect the growth kinetics significantly.[8] Therefore, the gas hydrate growth can be expressed as a first-order reaction. Other authors correlated the pressure of the system[8,34] or the concentration of CO_2[35] with the growth kinetics. As our experiments give direct information about the molar fraction of hydrate x_H with time t, we can write

$$\frac{dx_H}{dt} = r(x_{H,max} - x_H(t)) \quad (6)$$

with the maximum molar fraction at the end of growth $x_{H,max}$ and the reaction constant r.

Integrating eq 6 yields

$$x_H(t) = x_{H,max} - (x_{H,max} - x_{H,0})\exp(-rt) \quad (7)$$

This model is also very similar to the widely used Avrami equation,[36−38] for the case that the Avrami constant, which is an indication for the dimensionality of the hydrate growth, is one.

Figure 7a shows the growth constant r fitted to eq 7 and the maximal molar fraction of the solid hydrate formed $x_{H,max}$ (Figure 7b) for different effective mole fractions of the dissolved salt.

The growth constant r shows no significant change with increasing effective mole fraction. The literature regarding this differs significantly. Abay et al.[10] report that the growth kinetics of sII gas hydrates are dependent on the hydrate formed and not on the additives. This is in accordance with other authors who found the growth rate not to be or only slightly influenced by the addition of salt.[11,39] On the contrary, different works state that the growth rate is lessened by the addition of sodium chloride.[8,35] According to the hydrate growth model of Englezos et al.,[40] the hydrate growth is described analogously to crystal growth and consists of the following two steps: diffusion of the gas molecules to a hydrate particle, followed by an adsorption reaction in which the gas molecule is incorporated in the crystal. This means diffusion limitation and reaction limitation contribute to the growth constant r. Dissolved salts alter the diffusion coefficient of carbon dioxide in brines.[41] As we assume that strong agitations overcome mass transfer limitations, changes in the diffusion coefficient should not affect the growth constant calculated here. Usually, the growth constant shows a dependence on the temperature,[40,42−44] although the alteration of the growth constant reported in the literature ranges from 15 to 60% for a temperature variation of 2−3 K. As the experiments in this study were performed within a temperature range of 6 K, the value of r would be expected to vary. As it is not sure how much r should vary, it is also possible that due to the rather large error bars, this trend is not detectable.

DOI: 10.1021/acs.jpcb.8b11040
J. Phys. Chem. B 2019, 123, 2354−2361

All presented measurements were performed in an agitated system, though without a study of the effect of the stirring rate on the formation kinetics.

In Figure 7b, $x_{H,max}$ is always smaller than 0.2, when according to Figure 6b, the evolution of x_H stagnates. Therefore, self-inhibition could explain the stagnation and not the complete conversion of water into hydrates. When a hydrate phase forms, the salt ions do not participate in the cage structure. Therefore, the salinity of the remaining liquid water-rich phase rises, resulting in a shift of the equilibrium conditions. We calculated the shifts in the formation temperature induced by the formation of a hydrate phase using the determined values of the maximum amount of hydrate formed $x_{H,max}$ and the correlation from Hu et al. for the calculation of the hydrate equilibrium temperatures. The highest shift in the equilibrium temperature is 3 K. As the subcooling of 9−9.5 K exceeds that value, it is unlikely that self-inhibition is the reason for the stagnation of hydrate formation. We speculate that the growth phase can be divided into two phases: The first one is reaction limited, and mass transfer limitations can be neglected as a lot of CO_2 molecules are dissolved in the liquid water-rich phase, and the sample is stirred vigorously. By the time a hydrate phase forms and grows throughout the sample, the stirrer is blocked and stops to rotate. Then, the second diffusion limited phase starts. Carbon dioxide has to diffuse through the hydrate slurry phase that is not stirred. This happens probably in time scales we did not examine. Therefore, we observed the stagnation of hydrate formation after 30 min in our experiments.

$x_{H,max}$ shows a linear decline with the effective mole fraction of the dissolved salt. This is in agreement with previous works, in which the maximum gas uptake decreased with increasing salt concentration[8,9] or was lower in comparison to pure water[11,39,45] but without significant dependence on the mass fraction of the salt.

The diminution of $x_{H,max}$ is a direct result of the weakened hydrogen-bonded network and the decreased solubility of CO_2. As the interaction of water molecules between one another is disturbed by the presence of ions, it is more difficult to establish a hydrogen-bonded hydrate cage around CO_2 molecules. Additionally, less carbon dioxide molecules are available in solution for hydrate formation, leading to more water occlusions in the hydrate gel.

CONCLUSIONS

We presented an experimental Raman study on the parameters that lead to the inhibiting effect of thermodynamic inhibitors. It was shown that the disturbance of the hydrogen-bonded network characterized by the standard reaction enthalpy $\Delta_R h^0$ correlates directly with the effective mole fraction of salt in solution. We showed that the decomposition of the OH-stretching into five Gaussian peaks and bisecting at the isosbestic point yields different absolute values of standard reaction enthalpy $\Delta_R h^0$, but the percental diminution is approximately the same. Therefore, both methods are suitable to qualitatively describe the effect of thermodynamic inhibitors on the water-rich phase before the onset of hydrate formation. Additionally, the solubility of CO_2 in the aqueous solutions investigated was analyzed. The diminution of the solubility could also be correlated with the effective mole fraction, but a parameter that considers the size of the ions would be more suitable for a correlation.

Second, the effect of different thermodynamic inhibitors on the growth kinetics of CO_2 gas hydrates was examined. The reaction rate was not influenced by the presence of salts, whereas the maximum molar fraction of the solid hydrate formed decreased with increasing salt concentration.

AUTHOR INFORMATION

Corresponding Author

*E-mail: Andreas.Braeuer@tu-freiberg.de.

ORCID

Christine C. Holzammer: 0000-0001-8163-2840

Andreas S. Braeuer: 0000-0002-7816-4027

Notes

The authors declare no competing financial interest.

ACKNOWLEDGMENTS

The project leading to this result has received funding from the European Union's Horizon 2020 research and innovation programme under grant agreement no. 637654 (Inhomogeneities). Furthermore, we gratefully acknowledge the funding of the Erlangen Graduate School in Advanced Optical Technologies (SAOT) by the German Research Foundation (DFG) in the framework of the German excellence initiative.

REFERENCES

(1) Sloan, E. D. Fundamental Principles and Applications of Natural Gas Hydrates. *Nature* **2003**, *426*, 353−359.

(2) Hammerschmidt, E. Gas Hydrate Formations, a Further Study on their Prevention and Elimination from Natural Gas Pipe Lines. *Gas* **1939**, *15*, 30−34.

(3) McCain, W. D., Jr Reservoir-Fluid Property Correlations-State of the Art (includes associated papers 23583 and 23594). *SPE Reservoir Eng.* **1991**, *6*, 266−272.

(4) Yousif, M. H.; Young, D. B. A Simple Correlation to Predict the Hydrate Point Suppression in Drilling Fluids. *Proceedings of SPE/IADC Drilling Conference*; Society of Petroleum Engineers: Amsterdam, Netherlands, 1993; p 8.

(5) ØStergaard, K. K.; Tohidi, B.; Danesh, A.; Todd, A. C. Gas Hydrates and Offshore Drilling: Predicting the Hydrate Free Zone. *Ann. N. Y. Acad. Sci.* **2006**, *912*, 411−419.

(6) Hu, Y.; Lee, B. R.; Sum, A. K. Universal Correlation for Gas Hydrates Suppression Temperature of Inhibited Systems: I. Single Salts. *AIChE J.* **2017**, *63*, 5111−5124.

(7) Hu, Y.; Sa, J.-H.; Lee, B. R.; Sum, A. K. Universal Correlation for Gas Hydrates Suppression Temperature of Inhibited Systems: III. Salts and Organic Inhibitors. *AIChE J.* **2018**, *64*, 4097−4109.

(8) Woo, Y.; Lee, C.; Jeong, J. H.; Kim, D.; Lee, J.-W.; Yamamoto, Y.; Park, J.; Cha, M.; Yoon, J.-H. Clathrate Hydrate Formation in NaCl and $MgCl_2$ Brines at Low Pressure Conditions. *Sep. Purif. Technol.* **2019**, *209*, 56−64.

(9) Moeini, H.; Bonyadi, M.; Esmaeilzadeh, F.; Rasoolzadeh, A. Experimental Study of Sodium Chloride Aqueous Solution Effect on the Kinetic Parameters of Carbon Dioxide Hydrate Formation in the Presence/Absence of Magnetic Field. *J. Nat. Gas Sci. Eng.* **2018**, *50*, 231−239.

(10) Abay, H. K.; Svartaas, T. M.; Ke, W. Effect of Gas Composition on sII Hydrate Growth Kinetics. *Energy Fuels* **2011**, *25*, 1335−1341.

(11) Farhang, F.; Nguyen, A. V.; Hampton, M. A. Influence of Sodium Halides on the Kinetics of CO2 Hydrate Formation. *Energy Fuels* **2014**, *28*, 1220−1229.

(12) Holzammer, C.; Finckenstein, A.; Will, S.; Braeuer, A. S. How Sodium Chloride Salt Inhibits the Formation of CO_2 Gas Hydrates. *J. Phys. Chem. B* **2016**, *120*, 2452−2459.

(13) Holzammer, C.; Schicks, J. M.; Will, S.; Braeuer, A. S. Influence of Sodium Chloride on the Formation and Dissociation Behavior of CO_2 Gas Hydrates. *J. Phys. Chem. B* **2017**, *121*, 8330−8337.

DOI: 10.1021/acs.jpcb.8b11040
J. Phys. Chem. B 2019, 123, 2354−2361

(14) Carey, D. M.; Korenowski, G. M. Measurement of the Raman Spectrum of Liquid Water. *J. Chem. Phys.* **1998**, *108*, 2669−2675.
(15) Walrafen, G. E.; Hokmabadi, M. S.; Yang, W. H. Raman Isosbestic Points from Liquid Water. *J. Chem. Phys.* **1986**, *85*, 6964−6969.
(16) Schuster, J. J.; Guenther, A.; Wirth, K.-E.; Braeuer, A. Simultaneous Analysis of the Dispersed Liquid and the Bulk Gas Phase of Water Sprays Using Raman Spectroscopy. *Appl. Spectrosc.* **2016**, *70*, 1055.
(17) Bassing, D.; Braeuer, A. S. The Lag Between Micro-and Macro-Mixing in Compressed Fluid Flows. *Chem. Eng. Sci.* **2017**, *163*, 105−113.
(18) Li, H.; Stanwix, P.; Aman, Z.; Johns, M.; May, E.; Wang, L. Raman Spectroscopic Studies of Clathrate Hydrate Formation in the Presence of Hydrophobized Particles. *J. Phys. Chem. A* **2016**, *120*, 417−424.
(19) Harada, Y.; Miyawaki, J.; Niwa, H.; Yamazoe, K.; Pettersson, L. G. M.; Nilsson, A. Probing the OH Stretch in Different Local Environments in Liquid Water. *J. Phys. Chem. Lett.* **2017**, *8*, 5487−5491.
(20) Walrafen, G. E.; Fisher, M. R.; Hokmabadi, M. S.; Yang, W. H. Temperature Dependence of the Low-And High-Frequency Raman Scattering from Liquid Water. *J. Chem. Phys.* **1986**, *85*, 6970−6982.
(21) Geissler, P. L. Temperature Dependence of Inhomogeneous Broadening: On the Meaning of Isosbestic Points. *J. Am. Chem. Soc.* **2005**, *127*, 14930−14935.
(22) Smith, J. D.; Cappa, C. D.; Wilson, K. R.; Cohen, R. C.; Geissler, P. L.; Saykally, R. J. Unified Description of Temperature-Dependent Hydrogen-Bond Rearrangements in Liquid Water. *Proc. Natl. Acad. Sci. U.S.A.* **2005**, *102*, 14171−14174.
(23) Sun, Q. Local Statistical Interpretation for Water Structure. *Chem. Phys. Lett.* **2013**, *568*−*569*, 90−94.
(24) Sun, Q. Raman Spectroscopic Study of the Effects of Dissolved NaCl on Water Structure. *Vib. Spectrosc.* **2012**, *62*, 110−114.
(25) Hu, Q.; Guo, H.; Lu, W.; Lü, X.; Chen, Y.; Lin, L. Raman Spectroscopic Investigation on Aqueous NaCl Solutions at Temperatures from 273 To 573K: Effect of NaCl on Water Structure. *J. Mol. Liq.* **2014**, *199*, 83−87.
(26) King, M. B.; Mubarak, A.; Kim, J. D.; Bott, T. R. The Mutual Solubilities of Water with Supercritical and Liquid Carbon Dioxides. *J. Supercrit. Fluids* **1992**, *5*, 296−302.
(27) Teng, H.; Yamasaki, A.; Chun, M.-K.; Lee, H. Solubility of Liquid CO_2 in Water at Temperatures from 278 K To 293 K and Pressures from 6.44 MPa To 29.49 MPa and Densities of the Corresponding Aqueous Solutions. *J. Chem. Thermodyn.* **1997**, *29*, 1301−1310.
(28) Wiebe, R.; Gaddy, V. L. The Solubility of Carbon Dioxide in Water at Various Temperatures from 12 To 40° and at Pressures to 500 Atmospheres. Critical Phenomena*. *J. Am. Chem. Soc.* **1940**, *62*, 815−817.
(29) Pruppacher, H. R.; Klett, J. D. *Microphysics of Clouds and Precipitation*; Springer: Netherlands, 1996.
(30) Stamell, J. *Excel HSC Chemistry*; Pascal Press, 2011.
(31) Slusher, R. B.; Derr, V. E. Temperature Dependence and Cross Sections of Some Stokes and Anti-Stokes Raman Lines in Ice Ih. *Appl. Opt.* **1975**, *14*, 2116−2120.
(32) Plakhotnik, T.; Reichardt, J. Accurate Absolute Measurements of the Raman Backscattering Differential Cross-Section of Water and Ice and its Dependence on the Temperature and Excitation Wavelength. *J. Quant. Spectrosc. Radiat. Transfer* **2017**, *194*, 58−64.
(33) Sloan, E. D.; Koh, C. *Clathrate Hydrates of Natural Gases*, 3rd ed.; CRC Press, 2007.
(34) ZareNezhad, B.; Montazeri, V. Development of a High Efficient Gas to Hydrate (GTH) Conversion Process Using SDS Kinetic Promoter for Maximizing the CO_2 Recovery with Minimum Energy Consumption. *Energy Convers. Manage.* **2014**, *79*, 289−293.
(35) Sabil, K. M.; Duarte, A. R. C.; Zevenbergen, J.; Ahmad, M. M.; Yusup, S.; Omar, A. A.; Peters, C. J. Kinetic of Formation for Single Carbon Dioxide and Mixed Carbon Dioxide and Tetrahydrofuran Hydrates in Water and Sodium Chloride Aqueous Solution. *Int. J. Greenhouse Gas Control* **2010**, *4*, 798−805.
(36) Kumar, A.; Khatri, D.; Lee, J. D.; Kumar, R. Crystallization Kinetics for Carbon Dioxide Gas Hydrate in Fixed Bed and Stirred Tank Reactor. *Korean J. Chem. Eng.* **2016**, *33*, 1922−1930.
(37) Luzi, M.; Schicks, J. M.; Naumann, R.; Erzinger, J. Systematic Kinetic Studies on Mixed Gas Hydrates by Raman Spectroscopy and Powder X-ray Diffraction. *J. Chem. Thermodyn.* **2012**, *48*, 28−35.
(38) Susilo, R.; Ripmeester, J. A.; Englezos, P. Methane Conversion Rate into Structure H Hydrate Crystals from Ice. *AIChE J.* **2007**, *53*, 2451−2460.
(39) Yang, S. H. B.; Babu, P.; Chua, S. F. S.; Linga, P. Carbon Dioxide Hydrate Kinetics in Porous Media With and Without Salts. *Appl. Energy* **2016**, *162*, 1131−1140.
(40) Englezos, P.; Kalogerakis, N.; Dholabhai, P. D.; Bishnoi, P. R. Kinetics of Formation of Methane and Ethane Gas Hydrates. *Chem. Eng. Sci.* **1987**, *42*, 2647−2658.
(41) Cadogan, S. P.; Hallett, J. P.; Maitland, G. C.; Trusler, J. P. M. Diffusion Coefficients of Carbon Dioxide in Brines Measured Using 13C Pulsed-Field Gradient Nuclear Magnetic Resonance. *J. Chem. Eng. Data* **2015**, *60*, 181−184.
(42) Clarke, M. A.; Bishnoi, P. R. Determination of the Intrinsic Kinetics of CO_2 Gas Hydrate Formation Using in situ Particle Size Analysis. *Chem. Eng. Sci.* **2005**, *60*, 695−709.
(43) Lee, J.-w.; Chun, M.-K.; Lee, K.-M.; Kim, Y.-J.; Lee, H. Phase Equilibria and Kinetic Behavior of CO_2 Hydrate in Electrolyte and Porous Media Solutions: Application to Ocean Sequestration of CO_2. *Korean J. Chem. Eng.* **2002**, *19*, 673−678.
(44) Malegaonkar, M. B.; Dholabhai, P. D.; Bishnoi, P. R. Kinetics of Carbon Dioxide and Methane Hydrate Formation. *Can. J. Chem. Eng.* **1997**, *75*, 1090−1099.
(45) Nguyen, N. N.; Nguyen, A. V. The Dual Effect of Sodium Halides on the Formation of Methane Gas Hydrate. *Fuel* **2015**, *156*, 87−95.

DOI: 10.1021/acs.jpcb.8b11040
J. Phys. Chem. B 2019, 123, 2354−2361